Solidification behaviour and phase constituents of cast Mg–Zn–misch metal alloys

L. Y. WEI
Department of Engineering Materials, Luleå University of Technology, S 971 87 Luleå, Sweden

G. L. DUNLOP
CRC for Alloy and Solidification Technology (CAST), Department of Mining and Metallurgical Engineering, The University of Queensland, Queensland 4072, Australia

H. WESTENGEN
Norsk Hydro a.s., Research Centre Porsgrunn, P. O. Box 2560, N-3901 Porsgrunn, Norway

The solidification path and phase constituents of alloys in the magnesium-rich corner of the Mg–Zn–misch metal (MM) pseudo-ternary system have been investigated by a combination of differential thermal analysis, analytical electron microscopy and X-ray diffraction. The solidification behaviour diagram for this system was found to be dominated by a large two-phase (α-Mg plus T-phase) field in which the lowest eutectic temperature was $\sim 500\,^{\circ}C$. T-phase has a c-centred orthorhombic crystal structure and exhibits a wide range of stoichiometry. The interdendritic eutectic phase in the pseudo-binary Mg–MM system is $Mg_{12}MM$ which has the same bct structure as $Mg_{12}Ce$. The eutectic temperature here is 593 °C.

1. Introduction

The light alloy system Mg–Zn–rare-earth is of technological interest [1] because some alloys in this system exhibit good creep resistance at elevated temperatures. Because these alloys are generally used in the cast condition, it is of importance to understand the solidification process and establish the type of intermetallic phases that can be present. It is also important that this be done for alloys containing misch metal (MM) rather than individual rare-earth elements, as the low price of misch metal (approximate composition (wt %): 50 Ce, 25 La, 20 Nd, 2.7 Pr) can make it a more attractive alloying agent than individual rare-earth metals.

A study of the literature reveals that a variety of results has been obtained for different Mg–Zn–rare-earth systems. For instance, Dobatkina *et al.* [2] constructed the crystallization surfaces, and indicated the presence of two ternary phases, $(Mg, Zn)_{17}La_2$ and $Mg_{42}Zn_{53}La_5$, in the magnesium-rich region of the Mg–Zn–La system. Drits *et al.* [3] showed that Mg_9Nd, $MgNdZn_5$, $Mg_6Nd_2Zn_7$, $Mg_2Nd_2Zn_9$ and Mg_7Zn_3 could be in equilibrium with magnesium solid solution in the Mg–Zn–Nd system. In other work on the Mg–Zn–MM system, Petsol'd and Beyer [4] showed the existence of a pseudo-ternary phase $Mg_{20}Zn_5MM_2$.

In the present work, the solidification path and phase constituents of cast Mg–Zn–MM alloys were investigated by a combination of differential thermal analysis (DTA), analytical electron microscopy and X-ray diffraction (XRD).

2. Experimental procedure

Eight magnesium-rich alloys in the Mg–Zn–MM system with the composition shown in Table I were cast into permanent moulds.

Optical microscopy, electron microscopy, X-ray diffraction were employed to investigate the microstructure of these alloys. Differential thermal analysis at a cooling rate of about $1\,^{\circ}C/s^{-1}$ was used to register phase transformations taking place during the solidification process. Specimens for optical microscopy were prepared by standard techniques and subsequently etched in 1/3 HNO_3 in ethanol. Thin foils for transmission electron microscopy (TEM) were prepared by jet electropolishing in 1/3 HNO_3 in ethanol at 8–15 V and $\sim 0\,^{\circ}C$. The thin foils were subjected to a short ion-beam thinning operation of about 1 h with an incidence angle of $\sim 15^{\circ}$. This removed oxide layers which formed on the foil surfaces during electropolishing. The specimens were examined in a Jeol 2000FX TEM/STEM instrument with an attached Link AN 10000 EDX system. Microanalyses using the EDX system were made quantitative using the Link RTS-2/FLS computer program which compares spectra against standard peak profiles, applies the thin foil approximation, and makes corrections for absorption [5, 6]. Foil thickness were established using the

0022–2461

TABLE I Compositions of the investigated alloys (wt %)

Alloy	Composition
1	Mg–1.3MM[a]
2	Mg–20MM
3	Mg–20MM–10Zn
4	Mg–10MM–5Zn
5	Mg–5MM–2.5Zn
6	Mg–1.5MM–4Zn
7	Mg–1.5MM–8Zn
8	Mg–9Zn

[a] Misch metal is an alloy containing 50% Ce, 25 % La, 20 % Nd, 2.7% Pr.

TABLE II Reaction temperatures determined by DTA during solidification at 1 °C s^{-1}.

No.	Alloy	Reaction temperature (°C)			
		Peak 1	Peak 2	Peak 3	Peak 4
2.	Mg–20MM				593–593
3.	Mg–20MM–10Zn	590	560–510		
4.	Mg–10MM–5Zn	625	585–500		
5.	Mg–5MM–2.5Zn	645	580–497		
6.	Mg–1.5MM–4Zn	647	558–504		
7.	Mg–1.5MM–8Zn	625	480–447	346–316	
8.	Mg–9Zn	632		340–317	

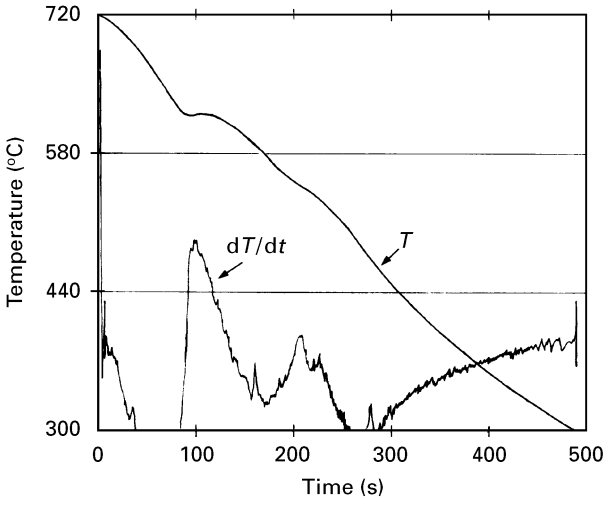

Figure 1 DTA curves for solidification Mg–10MM–5Zn. Curves for both T versus t and dT/dt versus t are shown.

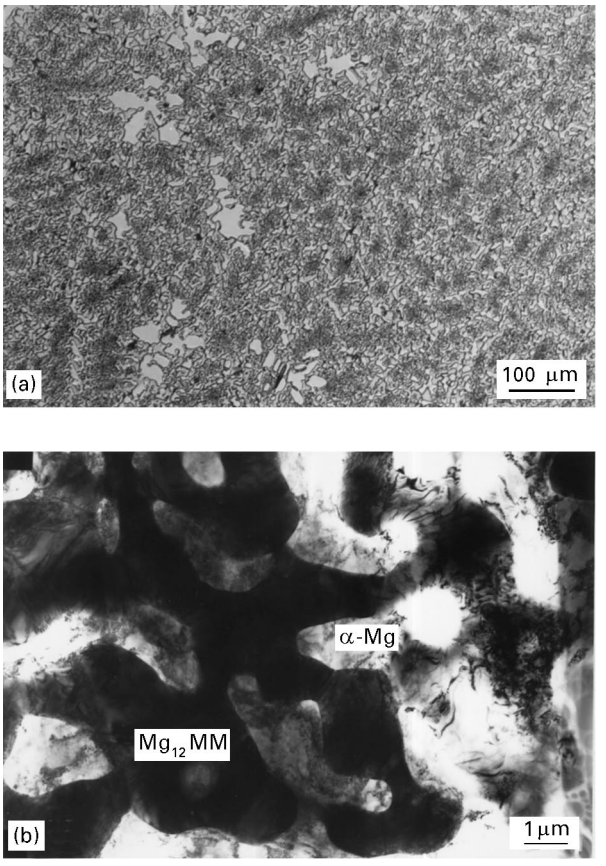

Figure 2 Solidification microstructure of the cast Mg–20MM alloy of near-eutectic composition. (a) Optical micrograph; note the small amount of primary α-Mg dendrites. (b) Transmission electron micrograph of the eutectic mixture of α-Mg plus $Mg_{12}MM$.

two-beam CBED technique [7]. The K_{xsi} value for magnesium was determined by measurements on an olivine standard mineral sample. Standard peak profiles were obtained from pure samples magnesium, zinc, La_2O_3, CeO_2 and Nd_2O_3. The camera length for electron diffraction patterns obtained from the specimens was determined from sharp diffraction rings on the diffraction patterns originating from a thin film of MgO on the foil surfaces. The estimated error limit for measurements on the diffraction patterns was about $\pm$ 0.05 mm leading to a relative error for the lattice parameters of about $\pm$ 1–1.5 %.

3. Results

3.1. Differential thermal analysis

A typical DTA cooling curve recorded during solidification is shown in Fig. 1. Inflections on cooling curves, that correspond to the solidification of various phases, appeared as peaks on the dT/dt (T is the temperature, t the time) curves. Temperature ranges for these solidification reactions are given in Table II.

Previous work [8] on alloys 6, 7 and 8 has indicated that peak 1 in Table II is due to the formation of primary α-Mg solid solution dendrites, i.e. L (liquid) → L + α-Mg and that peak 3 corresponds to the eutectic reaction whereby remaining liquid solidifies to α-Mg plus the intermetallic $Mg_{51}Zn_{20}$. The rare-earth element additions contained in alloys 6 and 7 resulted in the formation of the pseudo-ternary T-phase which solidified in the temperature range corresponding to peak 2.

The other "ternary" alloys (i.e. alloys containing both misch metal and zinc additions) had solidification peaks that seemed to correspond to the previously identified peaks for the solidification of the primary α-Mg phase and the pseudo-ternary T-phase. Only one peak appeared in the dT/dt curve for alloy 2 (Mg–20MM) and this corresponded to a substantial isothermal (593 °C) period in the cooling curve for the alloy.

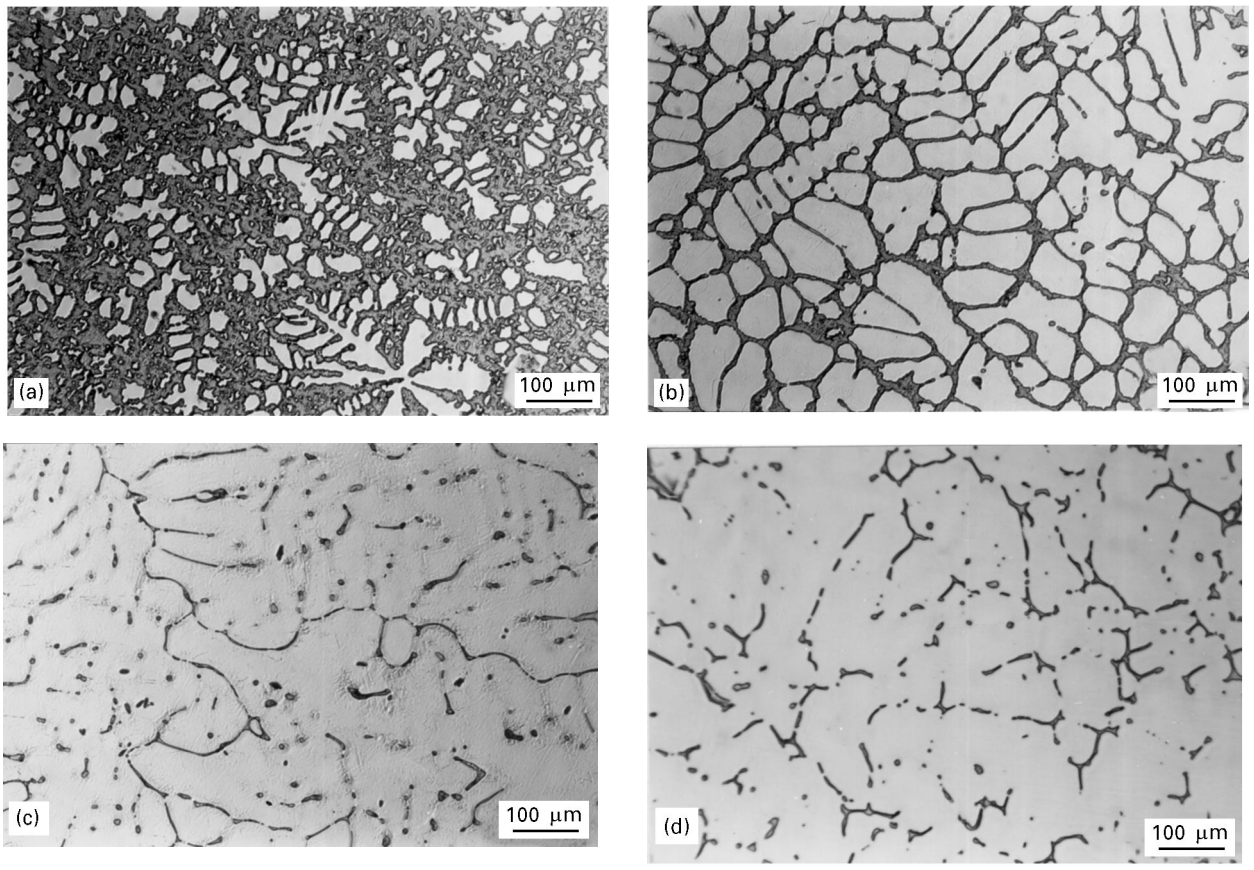

Figure 3 Solidification microstructures of cast Mg–MM–Zn pseudo–ternary alloys. (a) Mg–20MM–10Zn, (b) Mg–10MM–5Zn, (c) Mg–5MM–2.5Zn, (d) Mg–1.5MM–4Zn, (e) Mg–1.5MM–8Zn.

TABLE III Comparison of *d*-spacings for $CeMg_{12}$ [10] and $Mg_{12}MM$

h k l	*d*-spacing (nm)	
	$CeMg_{12}$	$Mg_{12}MM$
1 1 0	0.734	0.731
1 0 1	0.518	0.516
2 1 1	0.364	0.365
3 1 0	0.327	0.327
3 0 1, 0 0 2	0.298	0.298
3 2 1, 2 0 2	0.258	0.258

3.2. Eutectic transformation of the Mg–20MM alloy

The composition of this alloy was chosen with the expectation that it would be close to the eutectic composition for the Mg–MM pseudo-binary system because the Mg–Ce eutectic occurs at 19.4 wt % Ce [9]. The Mg–Ce eutectic temperature is 593 °C and this is the temperature at which the Mg–20MM alloy solidified. That the alloy composition was very close to the Mg–MM eutectic composition is shown by the optical micrograph in Fig. 2a. A few primary α-Mg dendrites were present in the microstructure, but otherwise the microstructure consisted of a typical two-phase eutectic mixture.

TEM confirmed the eutectic microstructure of the alloy (Fig. 2b) and the selected-area electron diffraction showed that the intermetallic phase in this microstructure had a b c t crystal structure with the following lattice parameters: $a = b = 1.03$ nm, $c = 0.60$ nm. This is similar to the $Mg_{12}Ce$ compound responsible for the Mg–Ce eutectic and therefore the phase is called here $Mg_{12}MM$. Interplanar *d*-spacings for this phase were obtained by X-ray diffractometry and are compared in Table III with those given by the ASTM powder diffraction file for $Mg_{12}Ce$. It can be seen that the correspondence between the two compounds is very close.

The composition of $Mg_{12}MM$ was determined by STEM/EDX to be (wt %): 66.7 ± 1.7 Mg; 13.2 ± 0.3 La; 17.7 ± 1.9 Ce; 2.5 ± 0.5 Nd. This corresponds to $Mg_{92}MM_8$ which, considering the accuracy of the measurements, is very close to $Mg_{12}MM$. Similar results concerning the crystal structure and composition of $Mg_{12}MM$ were obtained for the Mg–1.3MM alloy.

3.3. Solidification involving the pseudo-ternary T-phase

Optical metallography (Fig. 3) showed that all of the alloys that contained both zinc and misch metal (i.e. the pseudo-ternary alloys) were hypo-eutectic because primary α-Mg dendrites had formed in each of these during solidification. It can be seen from Fig. 3a that the composition of the Mg–20MM–10Zn alloys was only slightly hypo-eutectic with ~10 % of the microstructure being occupied by primary α-Mg dendrites. TEM showed that in all of these alloys the eutectic mixture of phases corresponded to α-Mg and the pseudo-ternary T-phase. Some typical micrographs of interdendritic grains of this phase in the Mg–5MM–2.5Zn alloy are shown in Fig. 4.

It has been shown elsewhere [8] that T-phase has a c-centred orthorhombic crystal structure with a C*m c m* space group and *m m m* point group. In the two pseudo-ternary alloys containing only 1.5 wt % misch metal (alloys 6 and 7) this phase had the following lattice parameters: $a = 0.96$ nm, $b = 1.12$ nm, $c = 0.94$ nm. The lattice parameters for T-phase in alloys 3, 4 and 5, where the MM/Zn ratio of 2 was much greater than in alloys 6 and 7, were found to be somewhat larger than for the two alloys containing 1.5 wt % misch metal: $a = 1.01$ nm, $b = 1.16$ nm, $c = 0.99$ nm.

The composition of T-phase in all of the pseudo-ternary alloys was determined using STEM/EDX. Typical spectra are shown in Fig. 5. The results of quantitative measurements, which in each case were made on a large number of different particles, are given in Table IV. It is clear from Table IV that T-phase can have a wide range of compositions. The rare-earth content of T-phase for alloys 3, 4 and 5 was virtually constant at ~28 wt % but the Mg/Zn content varied considerably. This consistency in total rare-earth content was reflected in consistent lattice parameter measurements for T-phase in these alloys. The rare-earth content of T-phase in alloys 6 and 7 was considerably lower at 22.5 wt % and here the lattice parameters were somewhat smaller.

3.4. High rare-earth content pseudo-ternary phase

During analysis of intermetallic particles in alloy 3 (Mg–20MM–10Zn) by STEM/EDX, it was found that a few of these particles had compositions out of keeping with the vast bulk of T-phase precipitates. Some typical compositions are given in Table V. The rare-earth content of these precipitates totalled ~38 wt %, but the Mg/Zn content varied considerably. The crystal structures of these precipitates was not determined and it is not known whether they were related to T-phase or had an entirely different structure.

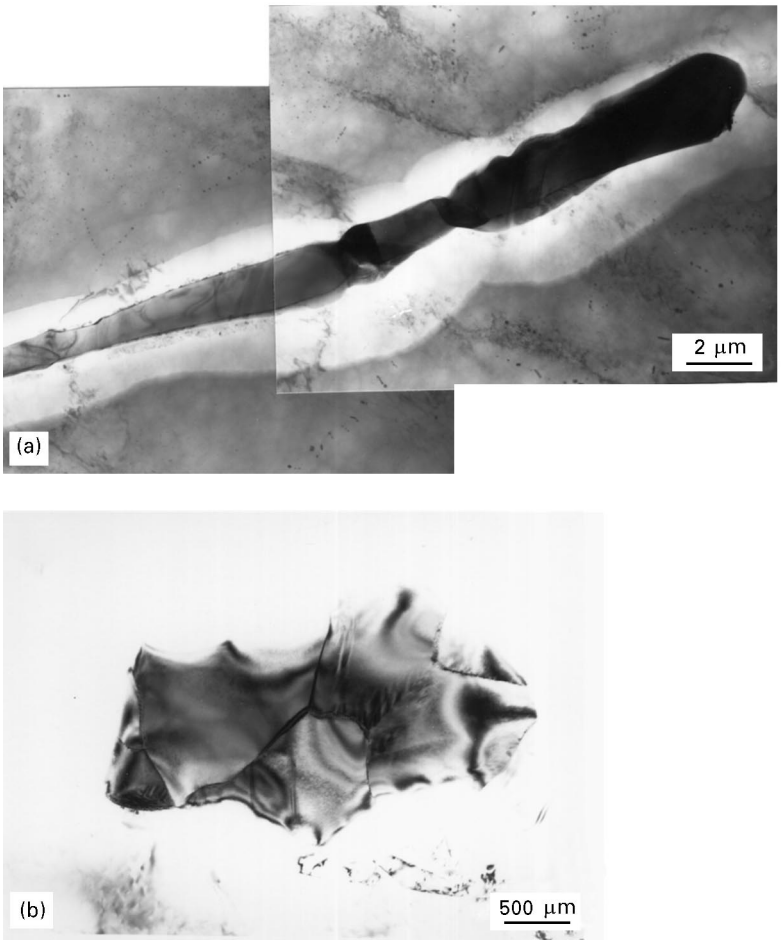

Figure 4 Interdendritic particles of T-phase in the Mg–5MM–2.5Zn alloy. Transmission electron micrographs of (a) a T-phase grain with a lamellar morphology, and (b) a group of T-phase grains.

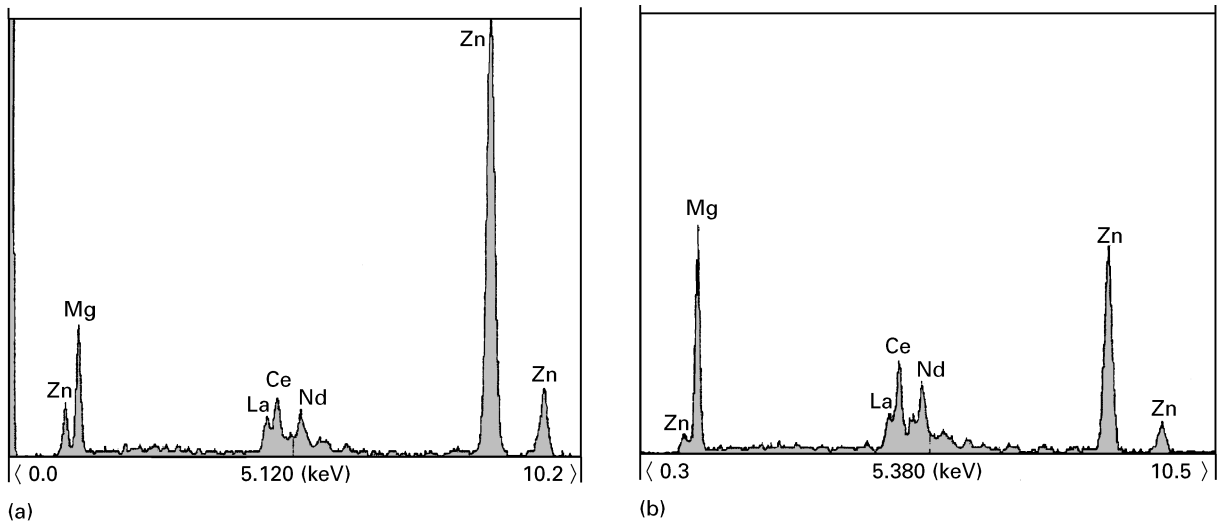

Figure 5 EDX spectra obtained from T-phase (a) in the Mg–1.5MM–8Zn alloy, (b) in the Mg–10MM–5Zn alloy.

TABLE IV Average chemical compositions (wt %) of T phase. The indicated error limits are the standard deviations of a number of different measurements.

Alloy	Mg	Zn	La	Ce	Nd
Alloy 4,5	52.4 ± 2.1	20.4 ± 1.5	8.4 ± 1.2	14.4 ± 1.2	4.4 ± 0.9
Alloy 3	43.3 ± 1.3	29.3 ± 2.9	9.3 ± 2.1	15.1 ± 1.4	4.0 ± 2.1
Alloy 3	35.2 ± 2.5	36.4 ± 0.8	7.8 ± 2.2	15.4 ± 2.0	5.2 ± 1.8
Alloy 6,7	25.8 ± 2.1	51.7 ± 1.9	8.0 ± 0.6	11.3 ± 1.0	3.2 ± 1.0

TABLE V Chemical composition (wt %) of some particles with high rare-earth content in alloy 3

Particle	Mg	Zn	La	Ce	Nd
1	34.1	28.4	11.4	19.0	7.1
2	26.7	34.8	10.8	23.2	4.5
3	18.0	43.5	12.5	20.4	5.6

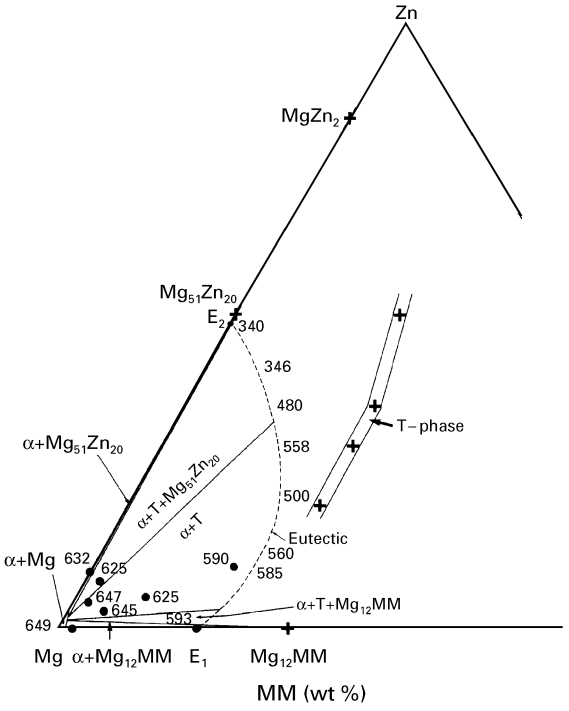

Figure 6 Approximate solidification behaviour diagram for solidification of alloys in the magnesium-rich corner of the Mg–MM–Zn pseudo-ternary system. Temperatures of the liquidus surface are indicated, as are different measured compositions of the pseudo-ternary T-phase.

4. Discussion

4.1. Solidification of pseudo-ternary Mg–MM–Zn alloys

Discussion of the solidification behaviour of magnesium-rich alloys in this system is best carried out with reference to the pseudo-ternary solidification behaviour diagram in Fig. 6 that has been drawn on the basis of the results present here. Because of the limited number of alloys that have been investigated, this diagram should only be considered as very approximate.

All of the alloys investigated were hypo-eutectic and the first solid phase to form during solidification was α-Mg solid solution which formed as primary dendrites. This corresponded to peak 1 in the DTA curves (see Table II). Depending upon alloy composition, the solidification began at temperatures in the range 647–590 °C, i.e. the liquidus temperatures for the investigated pseudo-ternary alloys lay within this range.

In the Mg–1.5MM–8Zn alloy the reaction of $L \rightarrow L + \alpha\text{-Mg}$ started at temperature 625 °C. The reflection between 480 and 447 °C resulted from the formation of the T-phase [8], and peak 3 that occurred between 346 and 317 °C corresponded to the formation of the pseudo-binary $MgZn_2$ (containing ~1.5 wt % rare-earth) and Mg_4Zn_7, etc., phases. These pseudo-binary phases could be the products of the decomposition reaction of $Mg_{51}Zn_{20}$ phase which had probably formed in the reaction of $L + \alpha\text{-Mg} + T \rightarrow \alpha\text{-Mg} + T + Mg_{51}Zn_{20}$ at about 346 °C.

With the exception of alloy 7 (Mg–1.5MM–8Zn) whose composition appeared to be in the three-phase α-Mg, T-phase, $Mg_{51}Zn_{20}$ phase field, the composition of the pseudo-ternary alloys all seemed to lie

within a large two-phase field with the as-solidified microstructures consisting of primary α-Mg dendrites and an interdendritic eutectic mixture of α-Mg and T-phase. According to the temperature range for peak 2 in the DTA curves, the highest eutectic temperature measured in this two-phase field was 585 °C and the lowest was ~500 °C.

The pseudo-ternary T-phase was found to have a wide range of compositions and the various compositions that were measured are indicated in Fig. 6. The considerable drop in eutectic temperatures along the eutectic line in the two-phase α-Mg + T region explains why a range of compositions for T-phase could occur in alloy 3 which had a large eutectic component.

4.2. The pseudo-binary Mg–MM eutectic

The approximate composition of misch metal used as a alloying addition in the present investigation was (wt %) 50Ce, 25La, 20Nd and 2.7Pr. It is perhaps reasonable to expect that intermetallic phases in the Mg–MM pseudo-binary system would be dominated by the major element in misch metal, i.e. cerium.

The intermetallic eutectic phase in the binary Mg–Ce system is $Mg_{12}Ce$ [9] and the corresponding phase in the Mg–La binary system is $Mg_{12}La$ [11], although earlier reports named Mg_9La as being responsible for the Mg–La eutectic [12]. Similarly, the eutectic phase in the Mg–Nd system is $Mg_{12}Nd$ [13]. The $Mg_{12}RE$ (rare-earth) intermetallic compounds have a b c t crystal structure and the lattice parameters of $Mg_{12}Ce$ have been given as $a = 1.033$ nm and $c = 0.596$ nm [12].

The present observation of an $Mg_{12}MM$ intermetallic phase with lattice parameter approximately the same as $Mg_{12}Ce$ would thus seem to be perfectly reasonable. The measured eutectic temperature of 593 °C was also the same as that for the Mg–Ce binary system [9].

4.3. The Mg–Zn binary eutectic

It has been shown previously that the intermetallic phase responsible for the Mg–Zn eutectic, which occurs at 340 °C is $Mg_{51}Zn_{20}$ [8, 14]. This phase was previously known as β phase, Mg_7Zn_3 [15]. $Mg_{51}Zn_{20}$ is not stable to room temperature but suffers eutectoidal decomposition in the temperature range 340–316 °C. Nevertheless, depending upon the rate of cooling, considerable amounts of $Mg_{51}Zn_{20}$ can be retained to room temperature. It was found that the dominant interdendritic phase in the cast Mg–9Zn alloy was $Mg_{51}Zn_{20}$ but, depending upon cooling rate, some of this can transform by eutectoid decomposition to a fine lamellar mixture of α-Mg and $MgZn_2$ (Laves phase) [8].

5. Conclusions

1. The solidification behaviour of a number of alloys in the magnesium-rich corner of the Mg–Zn–MM pseudo-ternary system has been established and an approximate solidification behaviour diagram has been drawn.

2. The magnesium-rich corner of the Mg–Zn–MM behaviour diagram is dominated by a large α-Mg plus T-phase region. The lowest eutectic temperature in this two-phase region is ~500 °C.

3. T-phase, which has a c-centred orthorhombic crystal structure, exhibits a wide range of compositions.

4. The intermetallic phase responsible for the eutectic in the Mg–MM pseudo-binary system is $Mg_{12}MM$. This phase has the same b c t structure as $Mg_{12}Ce$ and the eutectic temperature of 593 °C is the same.

Acknowledgements

Financial support from the Swedish Board for Technical Development and Norsk Hydro a.s. is gratefully acknowledged.

References

1. I. J. POLMEAR, "Light Alloys" (Chapman and Hall, London, 1989).
2. T. V. DOBATKINA, E. V. MURATOVA and E. I. DROZDOVA, *IZV. Akad. Nauka SSSR, Met.* **1** (1987) 205.
3. M. E. DRITS, E. M. PADEZHNOVA and N. V. MIKLINA, *ibid.* **3** (1974) 225.
4. F. PETSOL'D and B. BEYER, *Metal Sci. Heat Treat.* **13** (1971) 369.
5. J. I. GOLDSTEIN, J. L. COSTLEY, G. W. LORIMER and S. J. B. REED, in "Scanning Electron Microscopy/1977" Vol. 1 edited by O. Johari, (IITRI, Chicago, 1977) p. 315.
6. J. I. GOLDSTEIN, "Introduction to Analytical Electron Microscopy " (Plenum press, New York, 1979).
7. P. M. KELLY, A. JOSTSONS, R. G. BLAKE and J. G. NAPIER, *Phys. Status Solidi* (*a*), **31** (1975) 771.
8. L. Y. WEI, G. L. DUNLOP and H. WESTENGEN, *Metall. Mater. Trans.* **26A** (1994) 1947.
9. R. HULTGREN, P. D. DESAI, D. T. HAWKINS, M. GLEISER and K. K. KELLY, "Selected Values of the Thermodynamic Properties of Binary Alloys" (ASM, Metals Park, OH, 1973).
10. D. H. WOOD and E. M. CRAMER, *J. Less-Common Metals* **9** (1965) 321.
11. A. A. NAYEB-HASHEMI and J. B. CLARK, *Bull. of Alloy Phase Diag.* **9**(2) (1988) 172.
12. F. A. SHUNK (ed.), "Constitution of Binary Alloys", Second Supplement, (McGraw-Hill, New York, 1969) pp. 236, 471.
13. T. LYMAN (ed.), "Metals Handbook", Vol. 8, 8th edn. (ASM, Metals Park, OH, 1973) p. 314.
14. J. B. CLARK, L. ZABDYR and Z. MOSER, in "Binary Alloy Phase Diagrams", 2nd Edn, edited by T. B. Massalski, H. Okamoto, P. R. Subramanian and L. Kacprzak (ASM International, Ohio, 1990) pp. 2571–2.
15. J. B. CLARK and F. N. RHINES, *J. Metals* **209** (1957) 425.

Received 9 May 1995
and accepted 30 October 1996